

Relativistic beaming effects in the spectra of cores and hotspots in radio galaxies and quasars

C.H. Ishwara-Chandra^{1,2,3*} and D.J. Saikia^{1†}

¹ *National Centre for Radio Astrophysics, TIFR, Post Bag 3, Ganeshkhind, Pune 411 007, India*

² *Joint Astronomy Programme, Department of Physics, Indian Institute of Science, Bangalore, 560 012, India*

³ *Raman Research Institute, Sadashiva Nagar, Bangalore 560 080, India*

ABSTRACT

We present the results of multi-wavelength observations of cores and hotspots at L, C, X and U bands with the Very Large Array, of a matched sample of radio galaxies and quasars selected from the Molonglo Reference Catalogue. We use these observations to determine the spectra of cores and hotspots, and test the unified scheme for radio galaxies and quasars. Radio cores have been detected at all wavelengths in all the quasars in our sample, while only $\sim 50\%$ of the galaxies have detected cores in at least one wavelength. The degree of core prominence in this sample is consistent with the unified scheme for radio galaxies and quasars. A comparison of the distributions of the two-point spectral index of the cores in our sample of lobe-dominated quasars (LDQs) with a matched sample of core-dominated quasars (CDQs) shows that the distributions for these two classes are significantly different, consistent with the expectations of the unified scheme. The difference in the spectral indices of the two hotspots on opposite sides are also significantly larger for quasars than radio galaxies, as expected in the unified scheme. We also investigate the relationship between the spectral index of the hotspots and redshift or luminosity for our sample of sources.

Key words: galaxies: active - galaxies: nuclei - quasars: general - radio continuum: galaxies

1 INTRODUCTION

In the orientation-based unified scheme for radio galaxies and quasars, these objects are believed to be intrinsically similar, but appear to be different because of their different orientations to the line-of-sight. The quasars are oriented close to the line-of-sight, while the radio galaxies lie close to the plane of the sky, the dividing line being about 45° . There has been a reasonable degree of observational evidence in different wave bands in support of such a scheme (Scheuer 1987; Barthel 1989; Antonucci 1993; Urry & Padovani 1995).

In this paper we investigate the effects of relativistic beaming in the spectra of cores and hotspots in a matched sample of radio galaxies and quasars, to further test the unified scheme for these objects. We have attempted to determine the spectra of the cores using observations at two widely-spaced L-band frequencies, and at C, X and U bands. These observations represent one of the more extensive studies on the spectra of relatively weak cores in lobe-dominated radio sources. In an earlier study, Athreya et al. (1997) found

a high proportion of cores in their sample of high-redshift radio galaxies to have a steep radio spectrum between 4.7 and 8.3 GHz, and identified this with the optically thin part of the core spectrum. They also examined the spectra of core- and lobe-dominated quasars from available data in the literature, and suggested that the galaxy and quasar cores have intrinsically similar radio spectra. Lonsdale, Barthel & Miley (1993) found most of the radio cores in their sample of high-redshift, lobe-dominated quasars to have steep spectra between 5 and 15 GHz, indicating the presence of optically thin components. This is possibly due to the high emitted frequencies corresponding to these sources. We present the spectra of the cores in our sample and examine the effects of relativistic beaming in Section 4.

Relativistic effects in the spectra of hotspots in radio galaxies and quasars selected from the 3CR sample have been examined recently by Dennett-Thorpe et al. (1997, 1999). For the quasars they find that the spectrum of the high surface brightness region is indeed flatter on the jet side, but the spectrum of the low-brightness region is flatter on the side with the longer lobe. They interpret these results in terms of relativistic bulk motion in the spectra of the high brightness regions, and differential synchrotron

* E-mail: ishwar@ncra.tifr.res.in

† E-mail: djs@ncra.tifr.res.in

Table 1. Observing log

Array Conf.	Obs. band	Obs. Freq. MHz	Band-width MHz	Date of obs.
BnA	L	1365	50	1995 Sep 20
	L	1665	25	
CnB	C	4635	50	1996 Jan 20,31
	C	4935	50	
DnC	U	14965	50	1997 Sep 15, 16
DnC	U	14965	50	1997 Oct 3, 4, 12
BnA	X	8447	25	1997 Feb 3

ageing in the low-brightness regions. For the FR II galaxies, the spectral asymmetries appear to be uncorrelated with jet sidedness at all brightness levels, but appear to be related to relative lobe volume. In addition, earlier studies have shown that the less depolarized lobe has a flatter radio spectrum (Liu & Pooley 1991), and generally faces the radio jet (Laing 1988; Garrington et al. 1988; Garrington, Conway & Leahy 1991). We examine the effects of relativistic beaming in the spectra of the hotspots in our sample of radio galaxies and quasars using the scaled-array observations at L, C and U bands. These results are presented in Section 5. We also investigate any dependence of hotspot spectral indices on redshift or radio power.

In this paper, the sample and the observations are described in Section 2, while the observational results on the radio cores are presented in Section 3. The observed core prominence, the core spectra and their consistency with the unified scheme are presented in Section 4. The consistency of the hotspot spectra with the relativistic beaming effects and the unified scheme, as well as the dependence of hotspot spectra on redshift or luminosity are discussed in Section 5. The conclusions are summarised in Section 6.

2 SOURCE SAMPLE AND OBSERVATIONS

The sample and the selection criteria are discussed in detail in an earlier paper reporting the polarization properties of this well-defined sample of radio galaxies and quasars selected from the Molonglo MRC/1Jy sample (cf. Ishwara-Chandra et al. 1998, hereinafter referred to as IC98). Briefly, the sample consists of 15 quasars and 27 radio galaxies larger than about an arcminute in size with similar redshift, luminosity and projected linear size distributions. The observations were made with scaled arrays of the Very Large Array (VLA) of the National Radio Astronomy Observatory at 1.4 and 1.7 GHz (L-band), 5 GHz (C-band) and 15 GHz (U-band) with resolutions of $\sim 5''$, while observations at 8 GHz (X-band) have a resolution of $\sim 1''$. At 15 GHz, 14 quasars and 10 radio galaxies were observed, while at 8 GHz only those sources in the RA range 03h to 13h were observed due to scheduling constraints. The observing log is summarized in Table 1. All the data were calibrated and analyzed using the NRAO AIPS package. The images at X band and U band were corrected for primary beam attenuation. The U-band images have been restored with the same resolutions as the L- and C-band images, which are listed in Table 3 of IC98.

3 DETECTION OF RADIO CORES

All the quasars have detected radio cores at all wavelengths. In the case of radio galaxies, only two have reliable cores at all wavelengths, but many of them have weak cores in at least one wavelength. Of the 27 radio galaxies, 14 of them have a core detected in at least one wavelength, only 5 of which have a core flux density greater than 1 mJy. These 14 include two possible cores which are weak features seen in only the X-band images close to the positions of the optical galaxies. The peak flux densities of cores have been used to minimise contribution from nearby extended emission, and these values have been estimated using the AIPS task IMFIT. In the giant source 1025–229, the core flux densities have been estimated by fitting a gaussian to both the core and the nearby jet-like component in the L-, C- and U-band images. All the core flux densities estimated from the Gaussian fits are similar to the values at the pixel of maximum brightness near the optical position. Only those cores which could be clearly identified in the images have been listed in Table 2, which is arranged as follows. Column 1: Source name; column 2: optical identification where Q denotes a quasar and G a radio galaxy; column 3: redshift of the source; columns 4 to 9: peak flux densities of the cores at 1365, 1665, 4635, 4935, 8450 and 15000 MHz in units of mJy. In a few cases the core flux density could be significantly over-estimated due to extended diffuse emission in its vicinity. These have been marked with a superscript *d*. Columns 10 and 11: spectral indices between L and C bands, and between C and U bands, where the spectral index, α , is defined as $S(\nu) \propto \nu^{-\alpha}$. The spectral indices have been estimated using linear least square fits between the bands using the core flux densities at both the frequencies in the L and C bands. Cores with the superscript *d* have not been used. Column 12: the fraction of emission from the core at an emitted frequency of 8 GHz using the core spectral index determined from our observations and a spectral index of 1 for the extended emission. Column 13: N indicates that there is a note on the source in the text, while core? indicates a possible core. The positions of the optical objects have been listed by either McCarthy et al. (1996, hereinafter referred to as M96) if it is a galaxy, or by Kapahi et al. (1998, hereinafter referred to as K98) if it is a quasar. The typical errors in the optical positions are about $1.''5$ (M96) while for the quasars it is about $0.''5$ (K98). The positions of the new radio cores, which are not listed in K98, are presented in Table 3.

Notes on individual sources:

0148–297: The core is relatively weak at 4635 MHz; its position is the same as that of the stronger core at 15 GHz, and also consistent with the one seen at 1365 MHz.

0428–281: A weak radio core is detected at both the C bands as well as the X band. The radio positions of the core are the same in all the frequencies; but the core is about $5.''9$ from the optical position given by M96.

0551–226: The radio core detected at X band is about $2.''9$ from the optical position listed by M96.

1022–250: The possible radio core is about $2.''1$ from the position of the optical galaxy given by M96.

1107–218: The possible radio core is about $1.''6$ from the position of the optical galaxy given by M96.

Table 2. Observed and derived parameters of the radio cores

Source Name	Id	z	Flux density of the core					α_L^C	α_U^C	f_c	Notes	
			1365 MHz	1665 MHz	4635 MHz	4935 MHz	8450 MHz					15000 MHz
0017–207	Q	0.545	2.8 ^d	2.8	2.2	2.1		1.2	0.25	0.51	0.017	
0058–229	Q	0.706	4.3 ^d	3.8 ^d	2.1	2.4		1.0	0.51	0.71	0.020	
0133–266	Q	1.53	14.1	13.2	16.6	16.8			–0.17		0.10	
0148–297	G	0.41	1.9		0.4			2.5			0.00060	N
0428–281	G	0.65			~0.3	~0.2	~0.3				0.00074	N
0437–244	Q	0.84	16.9	15.2	12.8	12.5	10.5	4.4	0.21	0.92	0.089	
0454–220	Q	0.533	190.7	180.5	137.0	137.5	167.4	162.1	0.26	–0.15	0.26	
0551–226	G	0.8					0.4				0.0040	N
0938–205	G	0.371					0.6				0.0058	
0955–283	G	0.8				0.6	1.0				0.0042	
1022–250	G	0.34					~0.3				0.0039	N core?
1023–226	G	0.586					0.4				0.0050	
1025–229	Q	0.309	11.9	10.0	10.2	10.2	9.9	7.9	0.07	0.22	0.09	
1026–202	G	0.566			0.7	0.7	0.6	0.7			0.0040	
1029–233	G	0.611		0.8	0.5	0.4	0.5		0.56		0.0036	
1052–272	Q	1.103	2.3	2.1	1.8	2.0	1.2	1.2	0.13	0.40	0.0098	
1107–218	G	1.5					~0.3				0.0023	N core?
1126–290	G	0.41			1.9	1.7	1.4				0.0054	N
1226–297	Q	0.749	1.7	2.3	4.0	3.9	4.6	4.6	–0.61	–0.13	0.029	
1232–249	Q	0.352	17.5	14.7	11.2	10.6	10.0	8.2	0.34	0.25	0.023	
1247–290	Q	0.77	14.2 ^d	11.4 ^d	2.4	2.1	1.7	1.2	1.50	0.55	0.013	
1257–230	Q	1.109	16.2	16.4	15.4	15.0	10.1	8.1	0.06	0.55	0.055	
1358–214	G	0.5					0.6				0.0074	
2035–203	Q	0.516	34.7	38.1	40.0	38.7		29.7	–0.073	0.25	0.20	
2040–236	Q	0.704	119.1	116.4	91.7	90.3		74.3	0.22	0.18	0.740	
2118–266	G	0.343	27.2	28.6	51.6	51.8		47.5	–0.53	0.074	0.620	
2213–283	Q	0.946	38.3	40.7	54.2	54.1		56.7	–0.27	–0.04	0.19	
2311–222	G	0.434	2.4	1.6	1.9	1.7		1.1	0.11	0.43	0.0077	
2338–290	Q	0.446	30.4	31.9	40.4	40.8		64.5	–0.23	–0.40	0.40	

1126–290: The positions of the core at both the C bands and at the X band are consistent, but the core is about 12.''4 from the optical position given by M96. The position of the centroid of the optical galaxy measured from recent CCD observations of the field is RA: 11^h 26^m 26.^s434 and Dec: –29° 05' 02.''74 in B1950 co-ordinates. This is close to the position of the radio core.

4 RELATIVISTIC BEAMING IN THE CORES

To examine the consistency of the observations with expectations of the unified scheme, one needs to estimate reliably the flux density of the cores at the different frequencies. Since our observations at all the frequencies except at 8 GHz have been made with coarser angular resolution than is desirable, we have compared our measurements at 5 GHz with those of K98, which were also made at about 5 GHz but with an angular resolution of about 1''. The data are plotted in Figure 1 for all the objects in our sample for which core flux densities have been listed by K98. Since the epochs of the observations are separated by about 5 to 10 yr, there could be differences due to variability of the core flux density. It is, however, clear from the Figure that the values are con-

Table 3. Positions of radio cores

Source	RA (B1950)	DEC (B1950)
0148–297	01 48 19.679	–29 46 45.00
0428–281	04 28 17.326	–28 07 11.20
0551–226	05 51 17.431	–22 40 18.50
0938–205	09 38 30.873	–20 33 46.60
0955–283	09 55 36.536	–28 23 45.60
1022–250	10 22 57.085	–25 01 08.00
1023–226	10 23 10.267	–22 38 07.00
1026–202	10 26 35.174	–20 12 04.20
1029–233	10 29 12.174	–23 23 56.00
1107–218	11 07 44.986	–21 51 13.40
1126–290	11 26 26.443	–29 05 02.40
1358–214	13 58 47.273	–21 27 40.40

sistent over a wide range of flux density. Besides suggesting that the cores might be only weakly variable, this suggests that the effect of the coarser resolution is not significant at 5 GHz. At U band, it is likely to be even less significant, while at the L band we have identified those which are likely to be significantly affected by diffuse emission in the vicinity of the cores.

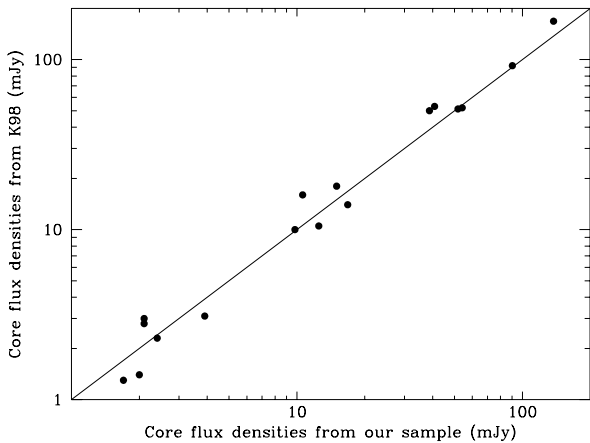


Figure 1. Plot of core flux densities at 4.9 GHz from K98 against the values estimated from our observations. Our estimates of core flux densities are from observations with an angular resolution of $\sim 5''$ compared to $\sim 1''$ by K98.

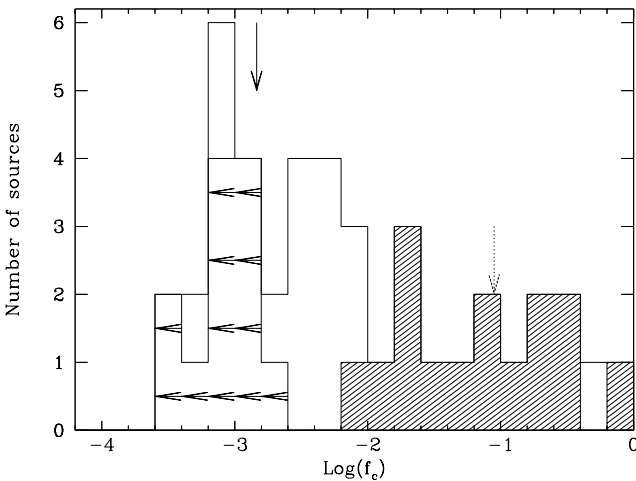


Figure 2. Distributions of f_c , the fraction of emission from the core at an emitted frequency of 8 GHz for the Molonglo radio galaxies and quasars in our sample. The quasars are shown hatched, while the upper limits are indicated by horizontal arrows. The median values of f_c for radio galaxies and quasars are shown by vertical solid and dotted arrows respectively.

4.1 Core prominence

In the orientation-based unified scheme for radio galaxies and quasars, the quasars are expected to show more prominent cores than radio galaxies due to the effects of relativistic beaming. All quasars have detected cores, compared to about 50% for the radio galaxies. The distributions of f_c , the fraction of emission from the core at an emitted frequency of 8 GHz, for our sample of radio galaxies and quasars is shown in Figure 2. The median values of the f_c are about 0.09 ± 0.04 for quasars and less than about 0.0015 ± 0.02 for the radio galaxies. Given the statistical uncertainties due to the small sample, these values are consistent with earlier estimates for the 3CR sample (cf. Saikia & Kulkarni 1994) as well as for a larger sample of Molonglo objects (K98). These values are

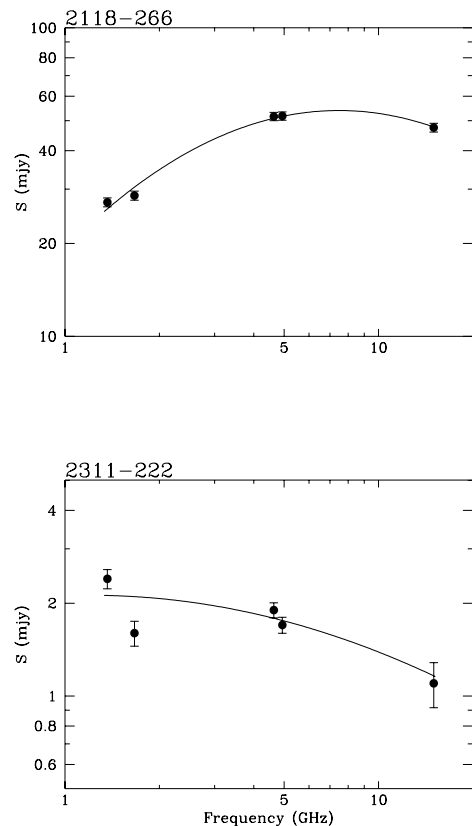


Figure 3. Observed spectra of two radio galaxy cores. The x-axis represents the frequency in GHz, while the y-axis represents the flux density in mJy. The source names are given in the top-left corner of each spectrum. The details of the fits are described in the text.

consistent with the unified scheme for radio galaxies and quasars.

4.2 Spectra of cores

Since only two of the galaxies have cores detected at all the observed wavelengths to determine reliably the spectra of the cores (Figure 3), we concentrate on the core spectra of the quasars to examine the effects of relativistic beaming. The spectra of all the cores in quasars are presented in Figure 4. In both the figures, the error bars correspond to 3% error on absolute flux density calibration and 1σ noise in the image. The spectra have been fitted by either a two- or three-degree polynomial, and in one source, 0454-220, by a straight line and a two-degree polynomial. The spectra are usually complex. The steep low-frequency spectra in the quasars 0058-229 and 1247-290 are possibly due to contributions from more extended emission near the core. The core in 1226-297 is a candidate GPS source (cf. O’Dea 1998) with a turnover frequency around 15 GHz, but higher frequency measurements would be required to confirm this.

In the observed spectra of the cores, the rest frequency in the frame of the quasar will appear shifted due to both cosmological redshift and Doppler shift due to relativistic beaming of the nuclear or core emission. The rest frequency will be shifted by an amount $\delta/(1+z)$ where $\delta = [\gamma(1 - \beta \cos\theta)]^{-1}$ is the Doppler factor, z the redshift of the

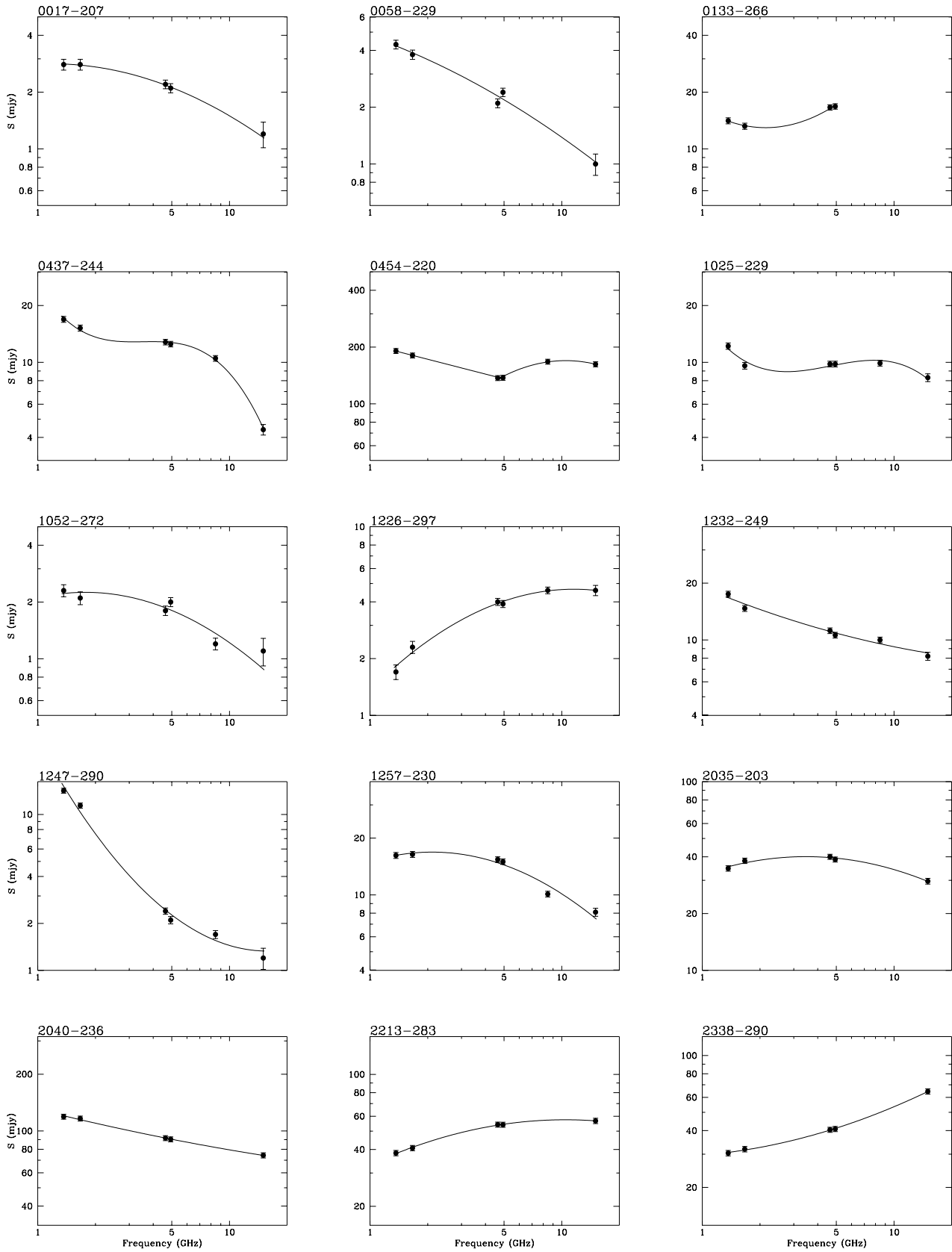


Figure 4. Observed radio spectra of quasar cores. The x-axis represents the frequency in GHz, while the y-axis represents the flux density in mJy. The source names are given in the top-left corner of each spectrum. The details of the fits are described in the text.

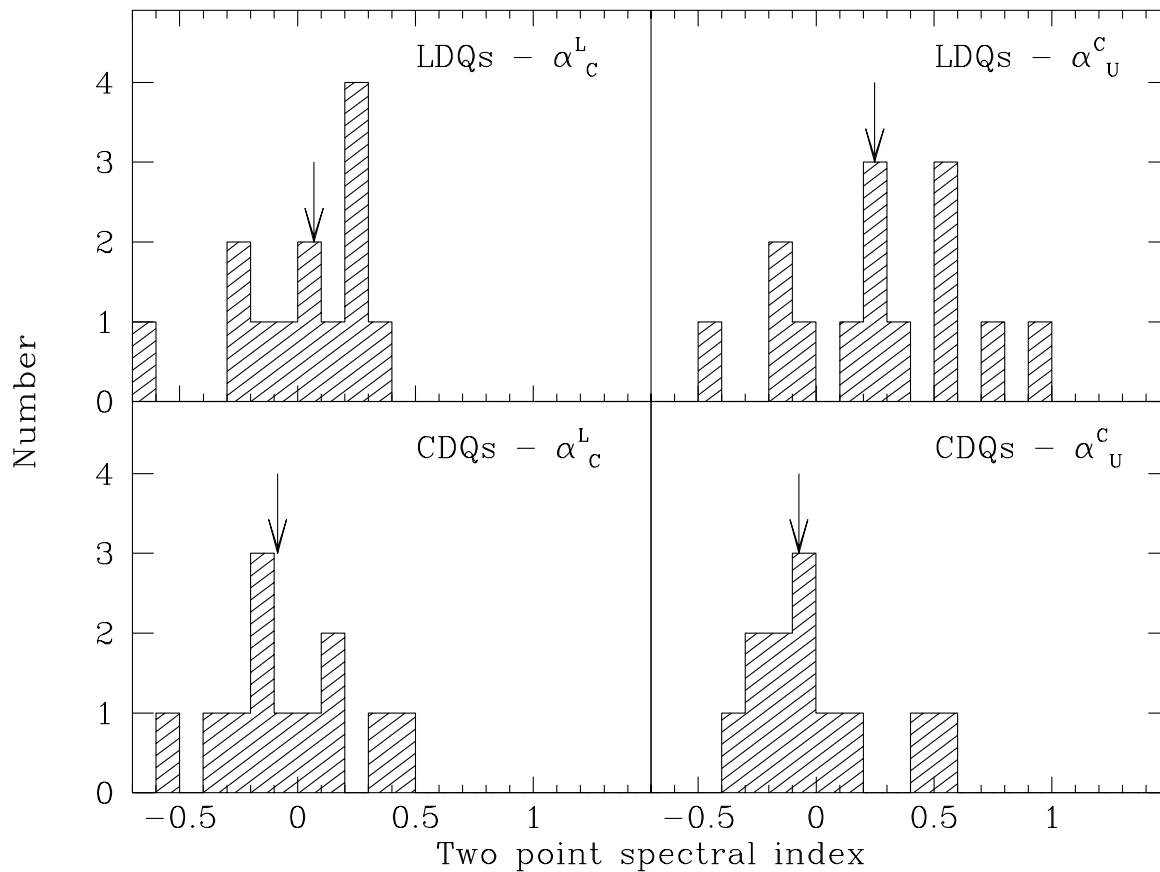


Figure 5. Comparison of the two-point spectral indices of lobe-dominated (LDQ) and core-dominated quasars (CDQ). The distributions of the spectral index between the L and C bands and between the C and U bands are shown in the left and right panels respectively. The median values of each distribution are shown by arrows.

source, γ the Lorentz factor, $\beta = v/c$, and θ is the angle of inclination of the jet or source axis to the line-of-sight. For fixed observed frequencies, ν_1 and ν_2 , the spectrum will be blue shifted for quasars, and in case of radio galaxies it will be generally redshifted. Assuming a Lorentz factor of 5, the Doppler factor δ for inclination angles of 15° , 30° and 60° , which correspond roughly to orientations of core-dominated quasars (CDQs), lobe-dominated quasars (LDQs) and radio galaxies, are 3.7, 1.3 and 0.4 respectively. Since we have determined the spectra of only 2 cores in radio galaxies, we concentrate on the quasars and compare their spectra with a sample of core-dominated quasars which have been observed at a single epoch by Saikia et al. (1998). The two samples have similar redshift distributions and have similar extended radio luminosity within a factor of ~ 2 . We present the distributions of spectral index between 1.4 and 5 GHz (α_c^L) and that between 5 and 15 GHz (α_c^U) for both the samples of LDQs and CDQs in Figure 5. These show that both α_c^L and α_c^U for CDQs are flatter compared to the corresponding values of LDQs, and the effect is more prominent in the high-frequency spectral index value (α_c^U). The median values of the two-point spectral index between 1.4 and 5 GHz and that between 5 and 15 GHz for LDQs are 0.07 ± 0.074 and 0.25 ± 0.085 respectively, while the corresponding values for the CDQs are -0.085 ± 0.073 and $-0.073 \pm$

0.068 respectively. A Kolmogorov-Smirnov test shows that the distributions of α_c^U for LDQs and CDQs are different at $> 99\%$ significance level, while that of α_c^L are different at less than about 80% significance level. These trends are consistent with the unified scheme since the spectra of CDQs will be blue shifted by a larger amount than LDQs due to relativistic beaming. The trend is more prominent at the higher frequency, possibly due to often being closer to the optically thin region of the synchrotron spectrum.

5 RELATIVISTIC MOTION IN THE HOTSPOTS

Estimates of hotspot advance speeds made from attributing arm-length asymmetries to geometrical projection and light-travel time effects range from about 0.2–0.5c (e.g. Longair & Riley 1979; Banhatti 1980; Best et al. 1995). Tighter constraints have been placed by Scheuer (1995) by noting that the approaching side can be identified in sources with radio jets (cf. Saikia 1981). He estimates an upper limit of $\sim 0.1c$. The properties of highly asymmetric or completely one-sided radio sources indicate hotspot advance speeds in the range of ~ 0.2 – $0.8c$ (Saikia et al. 1990). Proper motion studies of hotspots in compact VLBI-scale double radio sources yield values from about 0.05–0.5c (cf. O’Dea 1998).

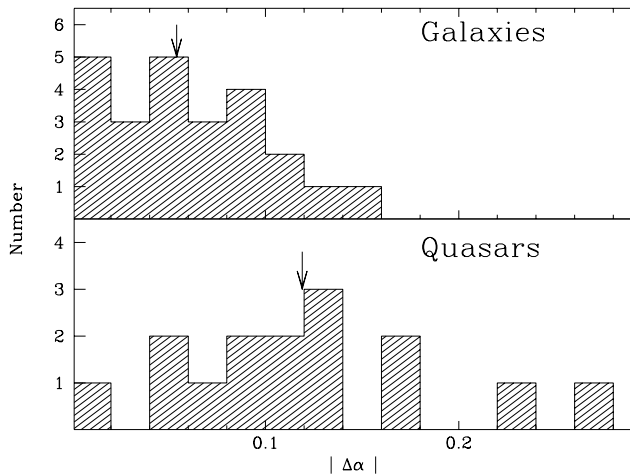


Figure 6. The distributions of the absolute difference in the hotspot spectral index $|\Delta\alpha|$ between 1.4 and 5GHz for the radio galaxies and quasars. The arrows indicate the median values.

5.1 Effects of relativistic motion in hotspot spectra

Assuming that the hotspots are advancing at mildly relativistic speeds, the observed spectral indices of the oppositely directed hotspots might appear to be different due to relativistic motion. If the hotspot spectra steepen towards higher frequencies, the approaching hotspot should exhibit a flatter spectrum over a fixed observed frequency range compared to the receding one due to relativistic Doppler effects. If the spectra are straight, any observed difference will reflect intrinsic differences in their spectra.

In the unified scheme for radio galaxies and quasars, the latter should exhibit a larger difference in the spectral indices of the hotspots on opposite sides due to smaller angles of inclination to the line-of-sight. Assuming a canonical spectrum for the hotspot, one might also be able to estimate the hotspot advance speeds for a sample of sources from the observed difference in hotspot spectral indices. For sources with detected radio jets, one can identify the approaching and receding hotspot. However, since we do not have detected radio jets in almost all the sources in our sample, we attempt such a study by examining the absolute difference in the hotspot spectral indices of the oppositely directed hotspots for the radio galaxies and quasars. In our study, we have defined the hotspot as the peak pixel in each lobe having surface brightness at least 10 times the weakest reliable flux density level. The number of sources with reliable hotspot flux densities at U band are small. Therefore we concentrate on the L- and C-band observations, but check for consistency with the U-band observations.

Our samples of radio galaxies and quasars are of similar redshift and luminosity, and therefore the effects of cosmological redshift are similar. The distributions of the absolute difference in the hotspot spectral index $|\Delta\alpha|$ between 1.4 and 5GHz is shown in Figure 6. There is a clear tendency for the quasars to show a larger spectral index difference than the radio galaxies. The median values of $|\Delta\alpha|$ are about 0.055 ± 0.0072 and 0.12 ± 0.015 for the radio galaxies and quasars respectively. A Kolmogorov-Smirnov test shows that the distributions are different at $> 99\%$ significance

level. The corresponding values for the spectral indices between C- and U-bands are 0.10 ± 0.015 and 0.19 ± 0.07 for the radio galaxies and quasars, again consistent with the trend expected in the unified scheme.

To understand the above difference in terms of relativistic beaming, we have considered a model hotspot spectrum with a curvature of 0.2 in the spectral index between each of the following successive pairs of frequencies, namely 0.408, 1.4, 5 and 15 GHz. There has been evidence in the past for curvature in the hotspot spectra. For example, Carilli et al. (1991) observed Cygnus A with an angular resolution of about $4.''5$ over a large frequency range and find evidence of spectral curvature in the hotspots. Wright, Chernin & Forster (1997) observed the hotspots in Cygnus A with an angular resolution of about $0.''4$ and also find evidence of spectral steepening. (See also Section 5.2 of this paper). The flatter spectra of the hotspots on the jet side can be better explained if the intrinsic spectra are curved downwards towards higher frequencies (Dennett-Thorpe et al. 1997, 1999). Assuming the above spectrum and an angle of $30\text{-}50^\circ$ for quasars and $50\text{-}90^\circ$ for radio galaxies, hotspot advance speeds in the range of $\sim 0.2\text{-}0.5c$ are required to produce the observed difference in the distributions. However, with our angular resolution of about $5''$, the corresponding sizes are typically about 25 kpc which is significantly larger than the sizes of hotspots in FR II radio sources (cf. Bridle et al. 1994; Fernini, Burns & Perley 1997; Hardcastle et al. 1998; Jeyakumar & Saikia 2000). Since the spectra of the extended emission tend to be steeper than the hotspots themselves, and the effects of relativistic beaming of hotspots are significant for quasars (Dennett-Thorpe et al. 1997, 1999), the relative contribution of the extended emission to our hotspot flux density within the $5''$ beam would tend to be larger for the receding hotspot compared to the approaching one. This would tend to increase the apparent difference in the spectral indices of the oppositely-directed hotspots, leading to a larger estimate of the hotspot velocity. Therefore, while our present estimates of $\sim 0.2\text{-}0.5c$ should be considered to be upper limits, a similar technique applied to higher resolution observations of hotspots should yield more reliable estimates of hotspot speeds. From our study the hotspot speeds appear to be at most mildly relativistic. It would also be important to study the curvature in the intrinsic spectra of the hotspots from higher-resolution observations.

If the sources are intrinsically symmetric and the effects of evolution of individual components with age are not dominant, one would expect the approaching hotspot, which has a flatter spectral index, to be farther from the nucleus and also brighter. However, we have shown in our earlier paper (IC98) that most of these sources appear to be evolving in an asymmetric environment. Nevertheless, for quasars where the effects of orientation are likely to be more significant, we do find a weak trend for the flatter hotspot to be on the longer side. This is true for 9 of the 14 quasars when one considers the spectral index between the L and C bands, and 7 of the 8 quasars for hotspot spectral indices between the C and U bands. The galaxies do not show any trend. We have also examined the relationship of the hotspot spectral indices with hotspot brightness ratio, but do not find any trend possibly due to the effects of environment as well as evolution of the individual components with age.

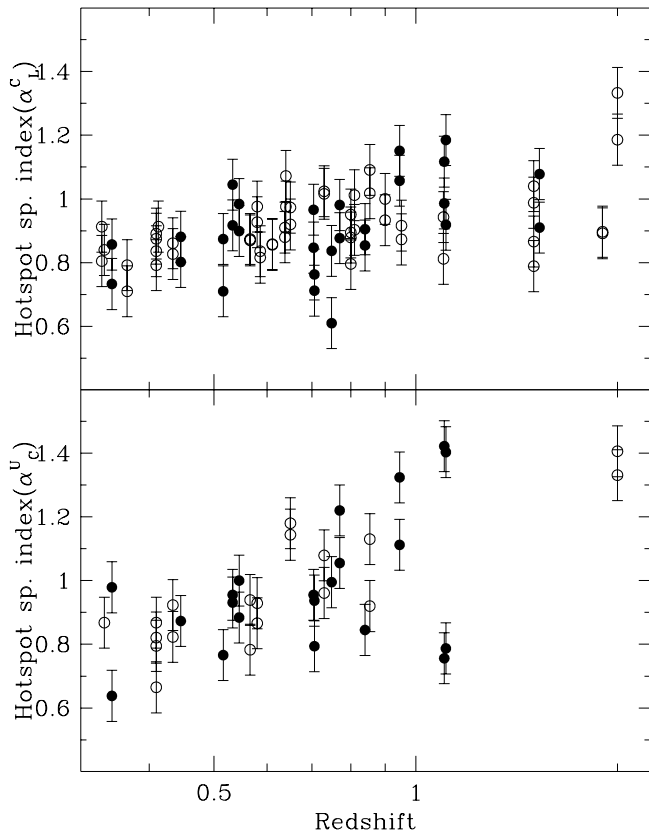


Figure 7. Plot of hotspot spectral index against the source redshift. The y-axis represents the hotspot spectral index between 1.4 and 5GHz (upper panel) and between 5 and 15 GHz (lower panel). Filled and open circles represent quasars and radio galaxies respectively.

5.2 Spectral index - redshift/luminosity relationship for hotspots

We have examined the spectral index - redshift/luminosity relationship for our sample using the spectra of the hotspots. At first glance, there appears to be a significant correlation of the spectral indices, $\alpha_{h,s}$, between 1.4 and 5 GHz, as well as between 5 and 15 GHz with redshift, z , the relationship being steeper for the higher frequency spectral index (Figure 7). A Spearman rank correlation test shows the relationship to be significant at a level >99 per cent. Since our sources are from a flux-density limited sample, redshift and luminosity are strongly correlated and we cannot distinguish between a dependence on either luminosity or redshift.

Steepening in the hotspot spectra towards higher frequencies, due to radiative losses can, in principle cause such a relationship since the emitted frequency will be higher for the higher redshift and hence more luminous objects. Inverse-Compton losses would also be important at higher redshifts. In a flux density limited sample, increased magnetic field for the more luminous objects will also increase the synchrotron emissivity, leading to an increase in the rate at which spectral steepening occurs (cf. Laing & Peacock 1980; Gopal-Krishna & Wiita 1990; Krolik & Chen 1991; Blundell, Rawlings & Willott 1999). Considering all the objects with $z < 1$, where the relationship is better defined, and

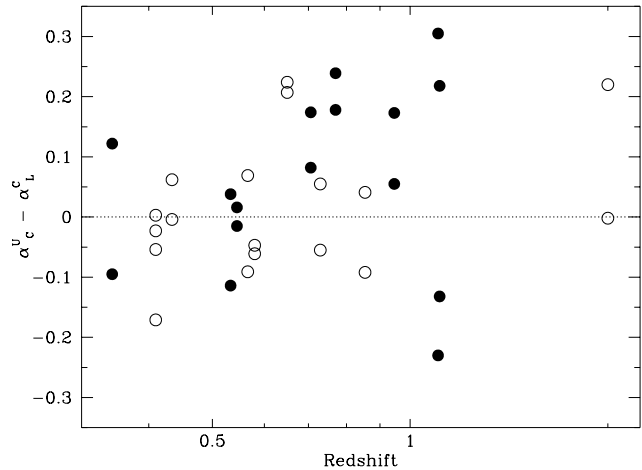


Figure 8. Plot of the difference of hotspot spectral index between 5 and 15GHz and that between 1.4 and 5GHz against the source redshift. Filled and open circles represent quasars and radio galaxies respectively.

dividing them into two equal groups in redshift the median values of $\alpha_C^U - \alpha_L^C$ are about 0 and 0.06. There is a weak trend for the high-frequency spectra to be steeper than the low-frequency ones as one goes toward higher redshifts upto $z \sim 1$ (Figure 8). Although we have plotted the observed spectral indices rather the ones in the rest frame of the source, the median redshift of the objects with $z < 1$ is about 0.6, so that the emitted frequencies for the low-frequency spectral index is about 2.2 and 7.8 GHz. The median values of α_L^C increase from about 0.8 to 1 as the redshift increases from about 0.3 to 1. This range is larger than the observed degree of spectral curvature, indicating that the correlation is not merely due to K-correction factors alone. This is consistent with earlier suggestions for the α -P relationship using the integrated spectra of the sources (cf. Lacy et al. 1993; van Breugel & McCarthy 1989).

However, while investigating the α - z relationship for hotspots one needs to consider the linear resolutions of the observations which are likely to be coarser at higher redshifts, leading to increased lobe contamination with increasing redshift. We have plotted the physical area of the restoring beam, A_b , for each source as a function of redshift, and have examined the $\alpha_{h,s}$ - z relationship for sources in restricted ranges of A_b as shown in Figure 9. We first consider the spectral indices between L and C bands where there are a larger number of sources. The slopes of the $\alpha_{h,s}$ - z relationship for sources with $800 < A_b < 1300 \text{ kpc}^2$, $1300 < A_b < 2000 \text{ kpc}^2$ and $2000 < A_b < 2800 \text{ kpc}^2$ are 0.11 ± 0.08 , 0.21 ± 0.11 and 0.48 ± 0.16 respectively. For sources observed with the highest linear resolution, which has the minimum contamination from the extended emission, the $\alpha_{h,s}$ - redshift plot is relatively flat, while the slope increases for sources observed with larger physical beam areas. A similar trend is seen while considering the hotspot spectral indices between the C and U bands. The slopes of the $\alpha_{h,s}$ - z plot for the three ranges of beam areas are 0.47 ± 0.30 , 0.99 ± 0.26 and 0.90 ± 0.39 respectively, the errors being larger because of the smaller number of sources observed at U band. These trends suggest that the hotspot spectral indices, which are closely related to the

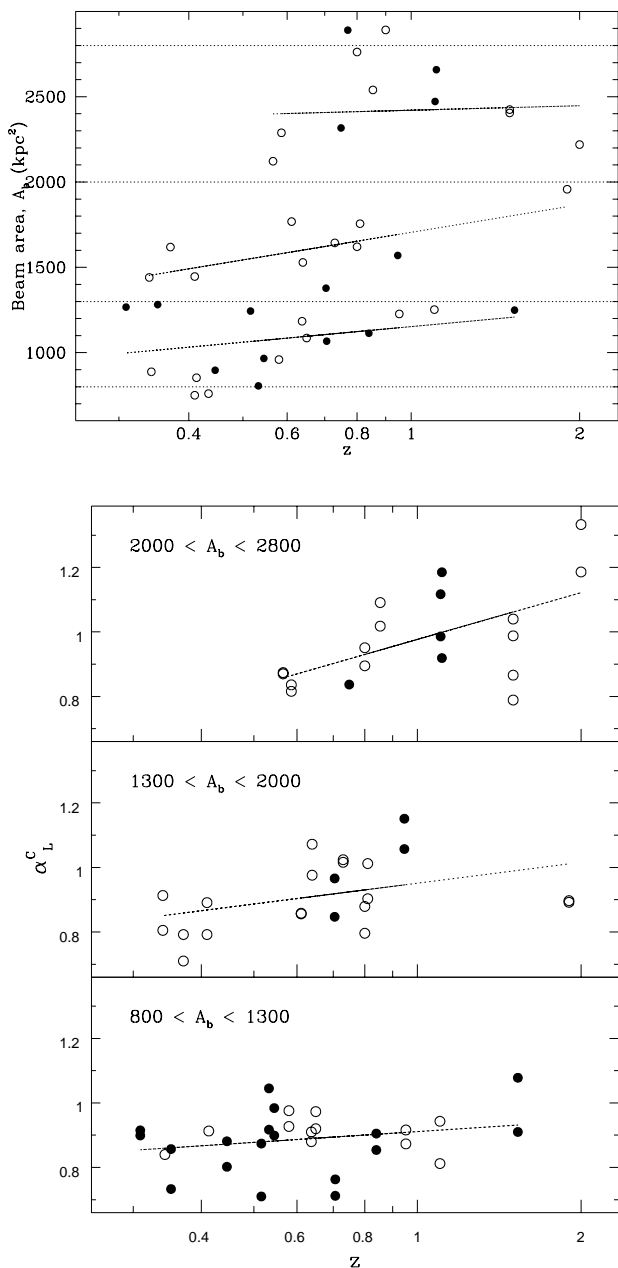


Figure 9. The area of the restoring beam, A_b , in units of kpc^2 plotted against redshift for all the sources (upper figure). The hot spot spectral indices between L and C bands are plotted against redshift for sources in the three restricted ranges of beam area marked in the upper figure. The ranges of A_b are labelled in each plot. The dashed lines indicate the least squares fits to the data. Filled and open circles represent quasars and radio galaxies respectively.

injection spectrum, are at best weakly dependent on redshift, while the observed relationship is largely due to the well-known relationship for the extended emission. It would be relevant to investigate the α_{hs} - z relationship with higher linear resolution than has been possible from our observations.

6 CONCLUDING REMARKS

We have studied multi-frequency radio spectra of cores and hotspots of a matched sample of radio galaxies and quasars. A comparison of the spectral indices of the cores of lobe-dominated and core-dominated quasars shows that the high-frequency spectral index of these two classes are significantly different. The difference can be understood in terms of Doppler effects and are consistent with the basic ideas of the unified scheme for radio galaxies and quasars.

The difference in the spectral indices of the hotspots on opposite sides of the nucleus is larger for quasars compared to radio galaxies, the median values of the difference being about 0.12 and 0.06 respectively. This difference could also be understood in terms of mild relativistic beaming of the hotspots. The hotspots have a curved radio spectrum steepening towards higher frequencies, possibly due to radiative losses. The difference is consistent with the unified scheme for radio galaxies and quasars and yields the velocity of advancement of the hotspots to be at most mildly relativistic.

We have investigated the correlation between spectral index and redshift/luminosity for the hotspots in our sample of sources. Although there appears to be a significant correlation, one needs to understand the effects of spectral steepening and lobe contamination in the hot spot spectral indices. Examining the low- and high-frequency spectral indices of the hotspots in our sample, the observed correlation cannot be due to the effects of K-correction alone. However, considering sources observed with similar linear resolutions in terms of beam areas, the α_{hs} - z relationship is flatter for the ones observed with the highest linear resolutions compared to those observed with coarser resolution. The hot spot spectral indices depend at best marginally on redshift for those observed with the highest linear resolutions, while for those observed with coarser linear resolutions the relationship appears similar to the well-known correlation for the extended emission. It would be interesting to investigate the spectral index - redshift relationship for hotspots using higher linear resolution than has been possible from our observations.

ACKNOWLEDGMENTS

We thank N.D. Ramesh Bhat, K.S. Dwarakanath, Gopal-Krishna, Vasant Kulkarni and Paul Wiita for their comments on the manuscript, and Ramesh Bhat for computational help. We are also indebted to an anonymous referee for very helpful and critical comments on the paper. The National Radio Astronomy Observatory is a facility of the National Science Foundation operated under co-operative agreement by Associated Universities Inc. We thank the staff of the Very Large Array for the observations.

REFERENCES

- Antonucci R., 1993, ARA&A, 31, 473
- Athreya R. M., Kapahi V. K., McCarthy P. J., van Breugel W., 1997, MNRAS, 289, 525
- Banhatti, D. G., 1980, A&A, 84, 112
- Barthel P. D., 1989, ApJ, 336, 606

- Best, P. N., Bailer, D. M., Longair, M. S., Riley, J. M., 1995, MNRAS, 275, 1171
- Blundell K. M., Rawlings S., Willott C. J., 1999, AJ, 117, 677
- Bridle A.H., Hough D.H., Lonsdale C.J., Burns J.O., Laing R.A., 1994, AJ, 108, 766
- Carilli C. L., Perley R. A., Dreher J. W., Leahy J. P., 1991, ApJ, 383, 554
- Dennett-Thorpe, J., Bridle, A. H., Scheuer, P. A. G., Laing, R. A., Leahy, J. P., 1997, MNRAS, 289, 753
- Dennett-Thorpe, J., Bridle, A. H., Laing R. A., Scheuer, P. A. G., 1999, MNRAS, 304, 271
- Fernini I., Burns J.O., Perley R.A., 1997, AJ, 114, 2292
- Garrington S. T. Leahy J. P., Conway R. G., Laing R. A., 1988, Nature, 331, 147
- Garrington S. T., Conway R. G., Leahy J. P., 1991, MNRAS, 250, 171
- Gopal-Krishna, Wiita P. J., 1990, A&A, 236, 305
- Hardcastle M.J., Alexander P., Pooley G.G., Riley J.M., 1998, MNRAS, 296, 445
- Ishwara-Chandra C. H., Saikia D. J., Kapahi V. K., McCarthy P. J., 1998, MNRAS 300, 269 (IC98)
- Jeyakumar S., Saikia D. J., 2000, MNRAS, 311, 397 (astro-ph/9904241)
- Kapahi V. K., Athreya R. M., Subrahmanya C. R., Baker J. C., Hunstead R. W., McCarthy P. J., van Breugel W., 1998, ApJS, 118, 327 (K98)
- Krolik J. H., Chen W., 1991, AJ, 102, 1659
- Lacy M., Hill G. J., Kaiser M.-E., Rawlings S., 1993, MNRAS, 263, 707
- Laing R. A., 1988, Nature, 331, 149
- Laing R. A., Peacock J. A., 1980, MNRAS, 190, 903
- Liu R., Pooley G. G., 1991, MNRAS, 249, 343
- Longair M. S., Riley J. M., 1979, MNRAS, 188, 625
- Lonsdale C. J., Barthel P. D., Miley G. K., 1993, ApJS, 87, 63
- McCarthy P. J., Kapahi V. K., van Breugel W., Persson S. E., Athreya R. M., Subrahmanya C. R., 1996, ApJS, 107, 19 (M96)
- O'Dea C. P., 1998, PASP, 110, 49
- Saikia D. J., 1981, MNRAS, 197, 11P
- Saikia D. J., Kulkarni V. K., 1994, MNRAS, 270, 897
- Saikia D. J., Junor, W., Cornwell, T. J., Muxlow T. W. B., Shastri P., 1990, MNRAS, 245, 408
- Saikia D. J., Holmes G. F., Kulkarni A. R., Salter C. J., Garrington S. T., 1998, MNRAS, 298, 877
- Scheuer P. A. G., 1987, in Zensus, J. A., and Pearson T. J., eds., Superluminal Radio Sources, Cambridge University Press, Cambridge, p. 104
- Scheuer P. A. G., 1995, MNRAS, 277, 331
- Urry C. M., Padovani P., 1995, PASP, 107, 803
- van Breugel W., McCarthy P. J., 1989, in Meurs E. J. A. & Fosbury R. A. E., eds, Extranuclear activity in galaxies, ESO Conference and Workshop Proceedings No. 32, ESO, p. 227
- Wright M. C. H., Chernin L. M., Forster J. R., 1997, ApJ, 483, 783